

Received 02.12.2019
Reviewed 05.03.2020
Accepted 25.05.2020

Structural, magnetic and adsorption characteristics of magnetically susceptible carbon sorbents based on natural raw materials

Christina SOLOVIY¹ ✉, Myroslav MALOVANYI¹, Ihor BORDUN²,
Fedir IVASHCHYSHYN², Anatoliy BORYSIUK¹, Yuriy KULYK³

¹ Lviv Polytechnic National University, Department of Ecology and Sustainable Environmental Management, Stepana Bandery Str., 12, Lviv, Lviv Oblast, 79000, Ukraine

² Czestochowa University of Technology, Faculty of Electrical Engineering, Czestochowa, Poland

³ Ivan Franko National University of Lviv, Faculty of Physics, Lviv, Ukraine

For citation: Soloviy Ch., Malovany M., Bordun I., Ivashchyshyn F., Borysiuk A., Kulyk Y. 2020. Structural, magnetic and adsorption characteristics of magnetically susceptible carbon sorbents based on natural raw materials. *Journal of Water and Land Development*. No. 47 (X–XII) p. 160–168. DOI: 10.24425/jwld.2020.135043.

Abstract

The article comprises synthesis of magnetically susceptible carbon sorbents based on bio raw materials – beet pulp. The synthesis was performed by one- and two-step methodology using FeCl_3 as an activating agent. X-ray diffraction methods showed an increase in the distance between graphene layers to 3.7 Å in biocarbon synthesized by a two-step technique and a slight decrease in inter-graphene distance to 3.55 Å for biocarbon synthesized by a one-step technique. In both magnetically susceptible samples, the Fe_3O_4 magnetite phase was identified. Biocarbon synthesized by a two-step technique is characterized by a microporous structure in which a significant volume fraction (about 35%) is made by pores of 2.2 and 5 nm radius. In the sample after a one-step synthesis, a significant increase in the fraction of pores with radii from 5 to 30 nm and a decrease in the proportion of pores with radii greater than 30 nm can be detected. Based on the analysis of low-angle X-ray scattering data, it is established that carbon without magnetic activation has the smallest specific area of $212 \text{ m}^2 \cdot \text{cm}^{-3}$, carbon after one-stage synthesis has a slightly larger area of $280 \text{ m}^2 \cdot \text{cm}^{-3}$, and after two-stage synthesis has the largest specific surface area in $480 \text{ m}^2 \cdot \text{cm}^{-3}$. The adsorption isotherms of blue methylene have been studied. Biocarbon obtained by two-step synthesis has been shown to have significantly better adsorption properties than other synthesized biocarbons. Isotherms have been analysed based on the Langmuir model.

Key words: *adsorption properties, biocarbon, iron (III) chloride, magnetic hysteresis, magnetically susceptible sorbent, porous structure*

INTRODUCTION

Unique physical and chemical properties of activated carbon materials provide the solution to many technical challenges associated with environmental and human security, the use of highly porous materials in energy, processing and chemical industries. Raw materials for the production of such carbon are wood and its waste, peat, coal and lignite, as well as various raw materials of organic origin [ABIOUE, ANI 2015; GONZALEZ-GARCIA 2018; IOANNIDOU, ZABANIOTOU 2007; KADIRVELU *et al.* 2003; XIAO-FEI *et al.* 2017; YAHYA *et al.* 2015]. Modern indus-

trial adsorbents are mostly used in two types – granular and powder. Granular adsorbents have the advantage that it is convenient for them to fill the adsorption columns without the need to separate the adsorbent from the solution. However, large particle sizes cause low kinetic characteristics of such adsorbent, and the granulation process not only adversely affects the adsorption properties, but also increases the cost of the adsorbent itself. Powder adsorbents look more promising in this regard. But in this case, the problem is the separation of the adsorbent from the solution. Due to the small particle size and density, which is commensurate with the density of water, the powder ad-

sorbent is difficult to separate by settling. In such cases filtering process is used, which, however, is a rather slow process. Alternative solution is to synthesize magnetically sensitive adsorbents, which can be separated by a magnetic separator from the solution with maintaining all the useful characteristics of powder adsorbents [KIM *et al.* 2011; WANG *et al.* 2012]. It is known that Ukraine has a well-developed sugar industry and is an exporter of this product. However, sugar production is a complex material and energy intensive production, in which the volumes of raw materials and auxiliaries are several times higher than the output of finished products [BUHAENKO 2007]. Thus, on average 1 t of sugar consumes 8–10 t of sugar beet, about 25–35 m³ of water, 0.6 t of calcareous stone, 0.53 t of conventional fuel. Thus, sugar production is a major source of secondary raw materials and wastes. At an average sugar yield of 10–12% to mass of processed beet, about 83% of fresh beet pulp, 5.4% molasses, 12% filtration sludge, 15% transport-washing sludge, up to 350% wastewaters etc. are formed. That is, the main solid by-product of sugar production is beet pulp. Pulp contains pectic substances, cellulose, sucrose, nitrogen compounds etc. 35–40% of it is used for livestock feed, 30% of pulp is dried, and the rest is often discarded in factory storages, thus losing much of the feed value and forming another waste – sour beet pulp water [BUHAENKO 2007].

The main areas of pulp utilization at present are its use as an active substance in the production of biogas, the production of pectin concentrate, pectin glue and dietary fibre from pulp as a fuel for the thermal power plant of a sugar plant [SPICHAK, VRATSKIY 2012]. However, these measures do not completely solve the problem of processing beet pulp. Therefore, the main purpose of the work was to obtain the AC from dried beet pulp, which would have magnetic properties, and to analyse possible ways to improve the characteristics of such carbon.

STUDY METHODS

METHODS OF AC SAMPLES PREPARATION

The raw material was washed in distilled water at room temperature until visually clear. It was dried in an air-drying oven at 100–110°C to constant mass. Part of the raw material was subjected directly to pyrolysis combined with the physical activation of the product by heating in a stainless steel tubular reactor under flow argon at 800°C. Activation was ensured by the supply of aqueous aerosol in argon from an ultrasonic aerosol generator to the reactor during carbonation. The gaseous reaction products were diverted by an argon stream through a water seal. The excess argon pressure in the reactor was kept at about 1 kPa, the flow rate was adjusted from 2 to 10 dm³·min⁻¹. In this way was obtained carbon, which we shall refer to hereinafter as AC0.

The rest of the raw material was subjected to pre-modification using FeCl₃ iron chloride. The ratio of feedstock – FeCl₃ was taken from the analysis of SAMAR and MUTHANNA [2012], where 1.5 g of iron chloride was taken per 1 g of feedstock. The synthesis of AC was carried out

at a temperature of 700°C and held at it for 90 min with vapour-gas activation using an ultrasonic aerosol generator according to the above modes. The carbon thus obtained will be referred to as AC1.

Chemical activation of natural raw materials is an important method of controlled change in the properties of the AC obtained from it. In the work with KOH modification, for example VERVIKISHKO *et al.* [2015] and DOBELE *et al.* [2012], the efficiency of two-stage carbon carbonization-activation is shown. This idea was also used to get AC with the modifier – FeCl₃ iron chloride. In the first stage of the synthesis, carbonation of beet pulp was carried out under an inert atmosphere (argon) at 400°C for 90 min. The char was soaked in an aqueous solution of iron (III) Chloride (approximately 10 g of anhydrous salt per 100 cm³ of water), kept for 24 h, and then dried in a drying oven at 100°C. In this case, the ratio of feedstock – iron chloride was maintained as in the previous case of one-stage synthesis of magnetic AC, that is, the reduction of the carbonate mass during the first stage of synthesis was taken into account. In the next stage, the modified FeCl₃ carbonate was activated in an inert atmosphere at 700°C for 90 min with the flow of argon in a water aerosol reactor. The result of the synthesis in this way gives us carbon, which we denote AC2.

The AC obtained by these syntheses methods was washed three times by boiling in distilled water for 30 min in a reflux vessel. The AC was then dried to constant mass at 100°C. For further experimental studies, the AC was crushed mechanically by grinding in a ceramic mortar.

METHODS OF EXPERIMENTAL STUDIES

A scanning electron microscope with a low vacuum camera and a REMMA-102-02 energy dispersive microanalysis system was used to obtain images of the synthesized carbon. This microscope is intended for the direct investigation of the various materials surface in the solid phase and the determination of their elemental composition using X-ray microanalysis by the quanta energy of characteristic X-ray radiation in low and high vacuum mode.

The X-ray diffraction curves of carbon materials were obtained using a DRON-3 diffractometer in Cu K_α radiation ($\lambda = 0.1542$ nm), monochromatized reflection from a pyrographite monocrystal (002) plane. Diffractograms measured in the continuous scan mode of the detector at a speed of 2 deg·min⁻¹ in the range of $2\theta = 5$ –120° diffraction angles. Processing of diffraction spectra (smoothing, subtraction of the background, determination of positions and half-widths of maxima, distribution of complex maxima into individual components) was performed using the DHN_PDS software package.

Measurement of small-angle X-ray scattering spectra (SAXS) was performed on a DRON-3 X-ray diffractometer in Cu-K_α radiation ($\lambda = 0.1542$ nm), monochromatized reflection from the plane (200) of a monocrystal LiF in the mode of passage of the X-ray beam through the sample. Primary and scattered beam collimators were used to limit the area of parasitic scattering of monocrystal – monochromator, input slits, and to reduce the intensity of back-

ground scattering in the air. The use of a collimation system allows the measurement of low-angle scattering spectra, starting from $s = 0.1 \text{ nm}^{-1}$, where $s = 4\pi \sin(\theta)/\lambda$ – the wave vector and 2θ is the scattering angle. A 0.1 mm slit was installed in front of the detector, which corresponds to the spatial separation of the $\Delta 2\theta = 0.03$ detector. The scattering was recorded in scan mode in 0.05° step, with an exposure time of $\tau = 125 \text{ s}$. In the area of the smallest scattering angles, a primary beam is placed on the scattered radiation, weakened by the absorption in the sample. In order to exclude the influence of the primary beam on the scattering intensity, the following ratio was used:

$$I^*(2\theta) = I_{\text{exp}}(2\theta) - T \cdot I_0(2\theta), \quad (1)$$

Where: $I^*(2\theta)$ = true scattering intensity, $I_{\text{exp}}(2\theta)$ = experimental scattering intensity, $I_0(2\theta)$ = the intensity distribution of the primary beam, $T = \frac{I_{\text{exp}}(0)}{I_0(0)}$ = transmission ratio (the fraction of the primary beam's intensity passing through the sample at the zero position of the detector). To determine the transmission coefficient, the scattering intensity measurements at the $2\theta = 0^\circ$ detector position were measured with the help of absorption filter method. In the obtained scattering intensity curves a collimation correction was made to the height of the detector receiving gap.

The study of adsorption of methylene blue was carried out according to the method described in [BESTANI *et al.* 2008], using a single-beam spectrophotometer SF-46 with a built-in microprocessor system, the absolute error limits in the measurement of transmittance by which in the 400–750 nm spectral range of not more than 0.5% nm. For measurements, cuvette with an optical travel length of 10 mm were used. When studying the adsorption properties of carbon materials it is necessary to deal with the suspension, where the role of the dispersed medium is a dye solution, and as a solid dispersed phase – carbon particles. To reduce the negative impact of particles that are additional scattering centres on the final determination of the concentration of the dye, an additional separation of such heterogeneous system was carried out by centrifugation for 10 min in an OPn-8 centrifuge at 8000 rpm mode.

Magnetic measurements were performed using a vibrating magnetometer [KONDIR *et al.* 2004]. The calibration of the magnetometer was carried out by comparison. Pure non-porous nickel with a density of $\rho = 8.9 \text{ g}\cdot\text{cm}^{-3}$ was used as the standard. The magnetization curves of the test samples were recorded in magnetic fields from $-300 \text{ kA}\cdot\text{m}^{-1}$ to $+300 \text{ kA}\cdot\text{m}^{-1}$.

The amount of magnetic phase in the obtained products was calculated according to the measurement of the specific saturation magnetization. During measurements in magnetic fields of insufficient intensity, the magnitude of the magnetization measured is not a unique function of the amount of ferromagnetic phase in the sample; it also depends on the phase structure (dispersion, stresses, etc.). Therefore, quantitative measurements of the saturation magnetization for phase analysis should be performed in strong fields sufficient for complete saturation. The problem of measuring the saturation magnetization is even more complicated when it comes to determining the prop-

erties of ferromagnetic particles in a non-magnetic matrix. In this case, the influence of the demagnetizing factor of the particles is significant, and only the use of strong fields allows to obtain reliable results. Therefore, the specific saturation magnetization was measured in a magnetic field of $800 \text{ kA}\cdot\text{m}^{-1}$, recommended by APAEV [1973].

All measurements were carried out on at least three samples. The measurement error was exclusively statistical in nature and did not exceed 5%.

RESULTS AND DISCUSSION

The scanning electron microscope (SEM) image of the carbon obtained from beet pulp is shown in Figure 1 a–c. The obtained AC mainly consists of a carbon base, but there is also the inclusion of other phases due to the presence of impurities in the feedstock. Most of the inclusions in Figure 1a are based on X-ray microanalysis mainly identified as SiO_2 and CaCO_3 phases. For Figure 1b and Figure 1c these inclusions have a more complex structure. The analysis of the total content of impurities (except oxygen) both in the carbon base and in the inclusions showed that for AC0 carbon it is about 8%, for AC1 carbon – 11.2%, and for AC2 carbon – 8.1%. The distribution of the basic elements in the synthesized biocarbons is shown in Figure 2. It shows that the content of elements such as Si, Mg, K, and Ca in the synthesis process decreases, with the last three elements being synthesized by the two-step method (AC2) most removed. Also the diagram in Figure 2 shows that the content of iron ions in AC2 is slightly higher than that of AC1 biocarbon in two-step synthesis, although the total impurity content is almost 30% lower.

X-ray diffraction patterns of the studied biocarbon samples are shown in Figure 3. On the diffractogram of the initial sample AC0 (Fig. 3a), a wide diffuse maximum is observed in the vicinity of the $2\theta = 28.8^\circ$ diffraction angle, which corresponds to the scattering from the graphite-like amorphous carbon phase with the distance between graphene layers $d_{(002)} = 3.60 \text{ \AA}$. On the diffuse halo, there is a clearly pronounced narrow maximum at $2\theta = 30.8^\circ$, which corresponds to the reflection from the planes (002) of polycrystalline graphite. It should also be noted that the presence of an additional diffuse maximum localized in the region of $2\theta \approx 10\div 20^\circ$ diffraction angles is probably caused by the formation of an amorphous carbon phase with a near atomic order different from the graphite-like amorphous phase. The diffraction pattern also exhibits a number of small crystalline phase peaks that are most likely associated with impurity elements present in the feedstock.

Concerning changes in the structural-phase state of biocarbons after chemical-thermal treatment, in the AC2 sample, the maximum position of the graphitic phase modifies slightly towards smaller scattering angles, which corresponds to an increase in the distance between graphene layers to $d_{(002)} = 3.70 \text{ \AA}$. Instead, the AC1 sample shows a slight decrease in inter-graphene distance to $d_{(002)} = 3.55 \text{ \AA}$. In addition, a number of additional peaks identified as Fe_3O_4 iron oxide (magnetite) phase are observed in AC1 and AC2 samples.

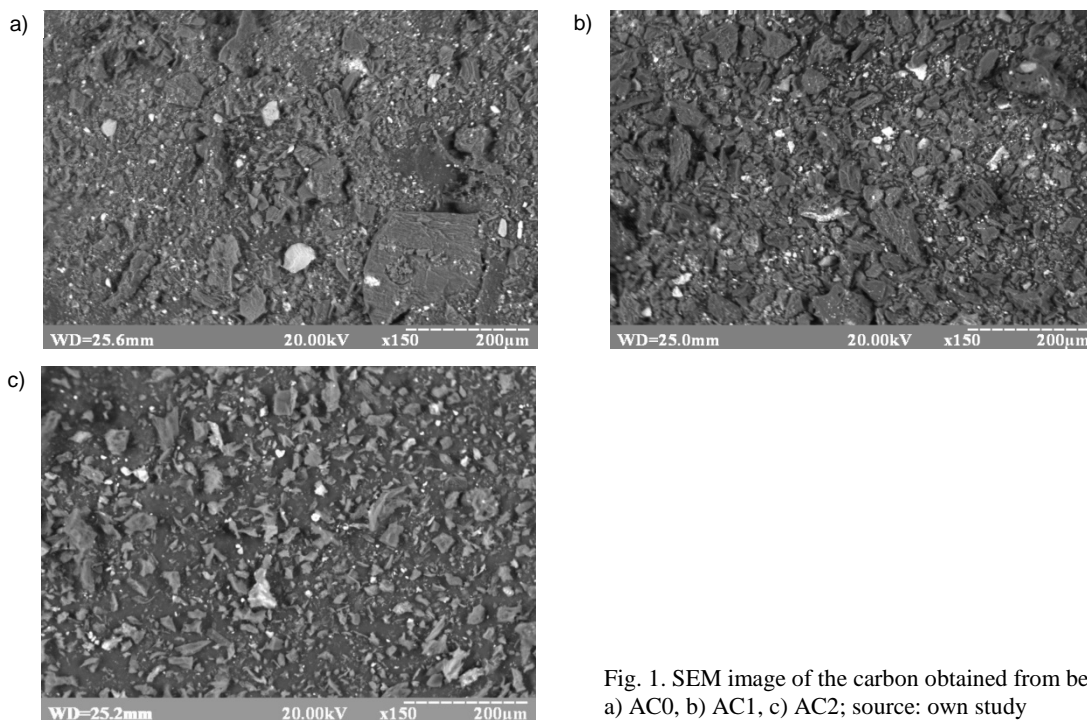


Fig. 1. SEM image of the carbon obtained from beet pulp: a) AC0, b) AC1, c) AC2; source: own study

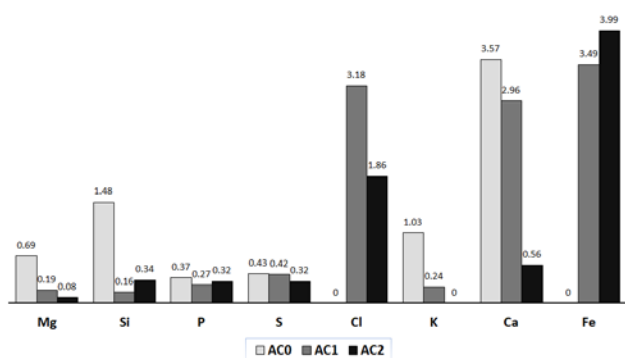


Fig. 2. Distribution of chemical elements in synthesized carbons in mass.%; source: own study

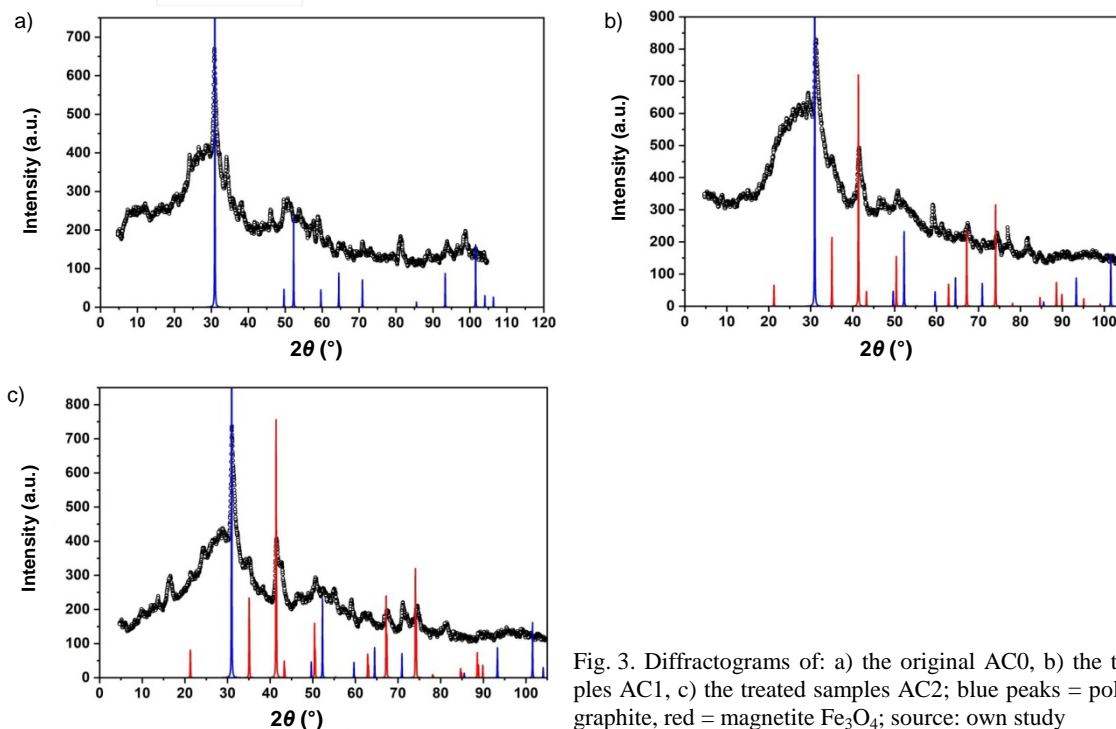


Fig. 3. Diffractograms of: a) the original AC0, b) the treated samples AC1, c) the treated samples AC2; blue peaks = polycrystalline graphite, red = magnetite Fe₃O₄; source: own study

Changes in the porous structure of biocarbons obtained from pulp feedstocks are provided by studies of the small-angle X-ray scattering (SAXS) spectra, which are shown in Figure 4. In the AC1 sample, there is an increase in the scattering intensity at the $s = 0.009 \div 0.07 \text{ \AA}^{-1}$ region, which corresponds to pore radii in the range from 4.5 to 35 nm. At the same time, in the regions of the smallest and largest scattering angles, the scattering curves of the AC1 and AC2 samples are practically the same. Comparison of the scattering spectra of the AC0 and AC2 samples reveals a significantly smaller value of the scattering intensity in the biocarbon from the feedstock in the $s > 0.035 \text{ \AA}^{-1}$ interval, which corresponds to the characteristic radii of the $R \approx \pi/s < 9 \text{ nm}$ pores. Thus, based on a qualitative comparison of low-angle scattering spectra, a significant increase in the volume fraction of medium-sized pores (4.5–35 nm) in the AC1 sample and a smaller proportion of pores less than 9 nm in the AC0 sample can be asserted.

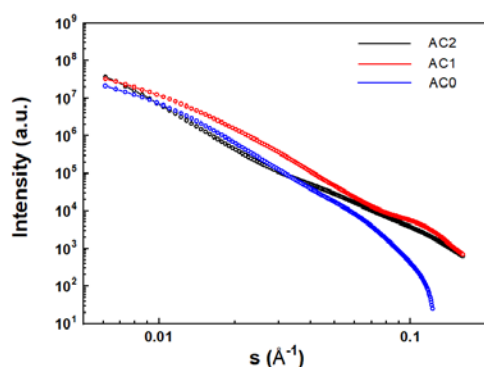


Fig. 4. Small-angle X-ray scattering spectra of carbonized samples from pulp raw materials; source: own study

To obtain quantitative information on the nature of pore distribution, the functions of the distribution of effective radii in the approximation of polydispersed spherical particles were calculated. Figure 5 demonstrates that there are significant differences in the distribution of pore radii, which confirm the previous qualitative estimates. The AC2 biocarbon obtained by two-step synthesis is characterized by a microporous structure in which a significant volume fraction (about 35%) is made by pores of 2.2 and 5 nm radii. A significant increase in the fraction of pores with radii from 5 to 30 nm and a decrease in the proportion of

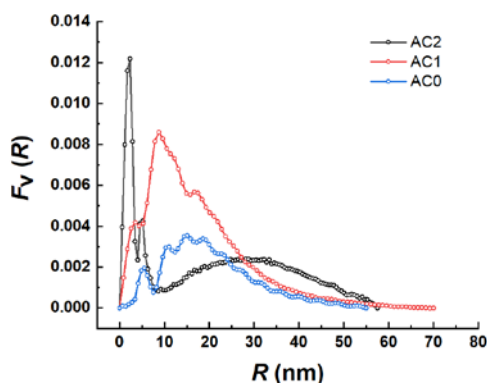


Fig. 5. Volumetric distribution functions for the radii $F_v(R)$ of biocarbons pores; source: own study

pores with radii greater than 30 nm can be detected in the AC1 sample. Instead, the comparison of the pore volume distributions in the AC2 and AC0 samples reveals a significant increase in the content of the pores by radii $R < 7 \text{ nm}$ and $R > 25 \text{ nm}$ after the activator is applied and only in the range from 7 to 25 nm, their proportion decreases slightly.

The analysis of the distribution functions of the radii of pores shows that the average radii in the samples AC2 and AC1 are almost indistinguishable (4.25 and 4.05 nm, respectively, Table 1), whereas in the sample AC0 this parameter reaches 20.8 nm. The analysis of the integral scattering characteristics (Porod invariant Q_p and Porod constant K_p) reveals significant differences of these values depending on the mode of sample processing. In the AC1 sample there is an increase of the Q_p invariant from 13.7 to 28.0 \AA^{-3} , which corresponds to an increase in the fraction of porous volume approximately 2 times compared to the original sample AC0. Instead, the value of the Porod constant K_p (Tab. 1) remains practically the same as that of AC2 due to the reduction of the content of the smallest pores by radii to 5 nm. As a result, a decrease in the specific surface area of the pores is observed. Significantly less value of both characteristics is found in biocarbon from AC0 feedstock. The small value of the constant K_p 0.09 \AA^{-4} is due to the small surface area of the pores due to the dominance of pores of large radii. Accordingly, AC0 biocarbon is characterized by the smallest value of the specific pore surface area (Tab. 1).

Table 1. The parameters of the biocarbons porous structure

Sample	R_C (nm)	Q_p (\AA^{-3})	K_p (\AA^{-4})	S ($\text{m}^2\text{-cm}^{-3}$)
AC2	4.25	19.3	0.280	451
AC1	4.05	28.0	0.250	280
AC0	20.8	13.7	0.09	212

Explanations: R_C = average radius, Q_p = Porod invariant, K_p = Porod constant, S = specific surface area.

Source: own study.

Comparison of the changes in the porous structure of the samples after the chemical-thermal treatment by the two-step method shows that this method effectively modifies the porous structure of the initial low-porous materials.

The adsorption value of methylene blue was calculated by the concentration difference before and after contact of its solution with the carbon adsorbent. Knowing the initial concentration of C_0 , the equilibrium residual concentration of solution C , the volume of solution V , and the mass of adsorbent m , one can calculate the amount of adsorbate. The amount of adsorption was calculated by the formula (2) [LOWELL, SHIELDS 1998]:

$$q_e = \frac{(C_0 - C) \cdot V}{m} \quad (2)$$

Where: q_e = the amount of adsorbate on carbon at equilibrium ($\text{mg}\cdot\text{g}^{-1}$); C_0 = initial concentration of stock solution ($\text{mg}\cdot\text{dm}^{-3}$); C = residual concentration of the equilibrium solution ($\text{mg}\cdot\text{dm}^{-3}$); V = volume of water solution (dm^3); m = amount of carbon used (mg).

Based on the obtained adsorption values, dependences $q_e = f(C)$ were constructed, that is, the adsorption isotherms shown in Figure 6.

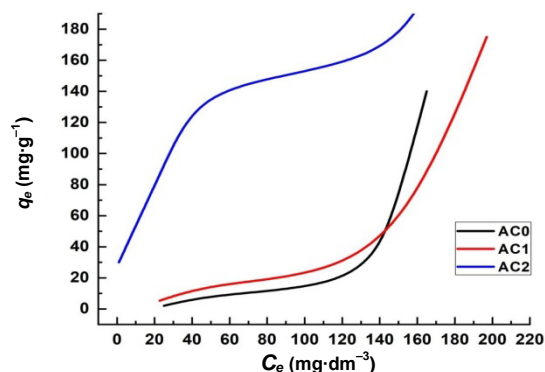


Fig. 6. Adsorption isotherms of methylene blue by synthesized biocarbons; source: own study

Adsorption isotherms are of great importance in describing how adsorbates will interact with carbon and are important in optimizing the use of carbon as an adsorbent. From Figure 6 it is clear that AC2 biocarbon has significantly better adsorption properties compared to AC0 and AC1. Analysing the shape of the isotherms in Figure 6, it can be said that all isotherms belong to the II type of adsorption isotherms, which indicates the presence of a certain number of meso- and macropores in addition to micropores.

Isotherms were analysed based on the Langmuir model. Langmuir equations are often used to describe experimental adsorption isotherms in the form [LOWELL, SHIELDS 1998]:

$$q_e = q_m \frac{K(C/C_0)}{1+K(C/C_0)} \quad (3)$$

Where: q_e = adsorption value ($\text{mg}\cdot\text{g}^{-1}$); q_m = maximum adsorption value ($\text{mg}\cdot\text{g}^{-1}$); C = residual concentration of the equilibrium solution ($\text{mg}\cdot\text{dm}^{-3}$); C_0 = initial concentration of stock solution ($\text{mg}\cdot\text{dm}^{-3}$); K = equilibrium constant of the interaction process of the adsorbate with the adsorbent – Langmuir constant ($\text{dm}^3\cdot\text{mol}^{-1}$).

It is convenient to use the linear Langmuir equation to analyse the experimental adsorption isotherms:

$$\frac{1}{q_e} = \frac{1}{q_m} + \frac{1}{Kq_m} \frac{C_0}{C} \quad (4)$$

By constructing adsorption isotherms in the $1/q_e = f(1/C)$ coordinates it is possible to determine the limiting amount of absorbed dye q_m by the porous carbon structure and Langmuir K constant. The values of the calculated parameters are given in Table 2. It also specifies the correlation coefficient r^2 for the Langmuir model.

Table 2. Adsorption parameters of methylene blue biocarbons by Langmuir model

Sample	q_m ($\text{mg}\cdot\text{g}^{-1}$)	K ($\text{dm}^3\cdot\text{mol}^{-1}$)	r^2
AC0	25.7	3.61	0.993
AC1	30.1	1.44	0.980
AC2	169.3	0.12	0.988

Explanations: q_m = maximum adsorption value, K = equilibrium constant of the interaction process of the adsorbate with the adsorbent (Langmuir constant), r^2 = correlation coefficient for the Langmuir model. Source: own study.

Since it is close to unite for all cases, this indicates that the Langmuir model is applicable to the adsorbent and adsorbate data.

From the Table 2 it is clear that AC2 biocarbon has the highest adsorption capacity among the studied carbon species. Comparing the data on the difference between the specific areas of the surface S_p (Tab. 1) and the difference in the values of the boundary absorption q_m (Tab. 2), the difference q_m between AC2 and AC0 and AC1 will be significantly larger. This difference may be due to the different content of the total number of surface oxygen-containing groups. This fact is reflected both in the adsorption rate and in the amount of absorbed dye, since in aqueous solution methylene blue has a positive charge and three basic amino groups that must be attracted to oxygen-containing surface groups on the surface of activated carbon [PAKHOVCHISHIN *et al.* 1991].

The adsorption process described by Langmuir can be expressed in characters [HSIEH, TENG 2000]:



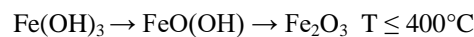
Where: A = the adsorbate molecule in the liquid phase; C^* = available adsorption centres; $C^*(A)$ = centres occupied by adsorbate.

The Langmuir constant K is the equilibrium constant of process 5). From the Table 2 it is clear that this constant decreases with increasing adsorption capacity of carbon. This means that AC2 carbon has a significantly smaller proportion of large pores, and micropores predominate [HSIEH, TENG 2000]. This conclusion is in good agreement with the results of the SAXS calculation shown in Figure 5.

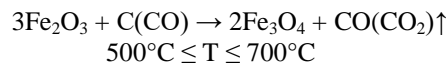
According to X-ray structural analysis, the magnetic properties of the synthesized carbon are due to the presence of Fe_3O_4 magnetite in their structure. In the process of carbonation of bio-raw materials, in the presence of iron (III) salts, processes occur that lead to the formation of iron oxides and the development of porosity [LIE *et al.* 2014; ZHU *et al.* 2016]. First of all, Fe^{3+} is hydrolysed to $\text{Fe}(\text{OH})_3$ at 350°C



Further heating in an inert atmosphere results in the dehydration and conversion of hydroxide to hematite Fe_2O_3 at 400°C



At higher temperatures (from 500°C to 700°C), Fe_2O_3 hematite is reduced to Fe_3O_4 magnetite by amorphous carbon and CO gas



By selecting the intensity of the argon stream, continuous removal of CO and CO_2 reaction products can be ensured as they are formed. The Fe_3O_4 magnetite can be further reduced by amorphous carbon to form metallic Fe.



In a number of papers (OLIVEIRA *et al.* [2009]; THEYDAN and AHMED [2012]) it has been reported that FeCl_3

promotes pore development in carbon-containing materials. Unfortunately, the mechanism of activation of FeCl_3 has not been sufficiently studied. On the other hand, the two reduction reactions given in equations (8) and (9) above can promote pore development in magnetic sorbent samples by converting C to CO and releasing carbon as CO, leaving certain cavities within the material structure.

Magnetic measurements show that the samples have a magnetic hysteresis (Fig. 7).

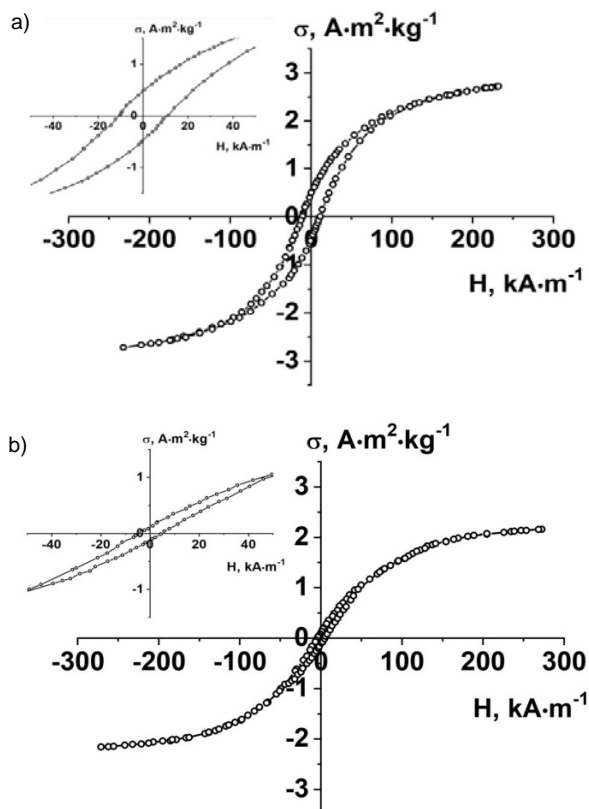


Fig. 7. Hysteresis loops of magnetic moment of biocarbons: a) AC1, b) AC2; σ = specific magnetization, H = magnetic field strength; source: own study

From the hysteresis loops were calculated the coercive force (H_c), the saturation specific magnetization (σ_s), the residual specific magnetization (σ_r), the relative residual magnetization (σ_r/σ_s) – Table 3.

Table 3. Magnetic characteristics of synthesized biocarbon

Sample	σ_s , ($\text{A}\cdot\text{m}^2\cdot\text{kg}^{-1}$)	H_c ($\text{kA}\cdot\text{m}^{-1}$)	σ_r/σ_s	Content of Fe_3O_4 (mass. %)
AC1	3.0	11.0	0.17	3.8
AC2	2.4	4.5	0.04	3.0

Explanations: σ_s = specific magnetization, H_c = coercive force, σ_r/σ_s = relative residual magnetization.
Source: own study.

According to the results of measuring the specific magnetization of the saturation of biocarbons, it is possible to determine the content of particles of carriers of magnetic moment – magnetite. To calculate it is necessary to know the magnitude of the specific magnetization of the saturation of the magnetite particles. The specific magnetization

of saturation of massive magnetite is $92 \text{ A}\cdot\text{m}^2\cdot\text{kg}^{-1}$ [COEY 2010]. Necessary for the calculation of the specific magnetization of the saturation of the particles of magnetite was chosen taking into account the phenomenon of reducing the magnetization of small particles with a decrease in their size [HUBIN *et al.* 2005]. According to the dependence of the coercive force on the particle diameter in the Fe_3O_4 [GOYA *et al.* 2003; YANG *et al.* 2008] dispersions for the measured values of the coercive force, the size of the magnetic moment carriers ranged from 30 nm for the AC2 sample to 50 nm for AC1. Taking from the above sources that the specified particle size corresponds to the average value of the specific saturation magnetization $80 \text{ A}\cdot\text{m}^2\cdot\text{kg}^{-1}$, the magnetite content was determined (Tab. 3). The values calculated in this way are smaller than those obtained from the energy dispersive X-ray microanalysis data. This situation may be due to the fact that X-ray microanalysis provides information about the surface layers of matter, since the bombardment of the object occurs by an electron beam. As a result, in addition to the brake continuous X-ray spectrum, we obtain a spectrum of characteristic radiation whose lines correspond to the chemical elements present in the substance. However, the penetration of the electron beam into the particle is small, in the order of micrometers or even less. Therefore, in the case of unequal distribution of elements in the particle with depth, the results of the three-dimensional (magnetic) and surface (X-ray) microanalysis may differ. Comparing the results presented in Figure 2 and in Table 3, we can conclude that in AC2 biocarbon, the magnetic fraction is more in the surface layers, and in AC1 it is more evenly distributed in depth.

CONCLUSIONS

1. In the sample of AC2 biocarbon synthesized by the two-stage technique, the X-ray diffraction studies showed an increase in the distance between graphene layers to $d_{(002)} \approx 3.70 \text{ \AA}$. Instead, the AC1 sample synthesized by the one-step technique shows a slight decrease in inter-graphene distance to $d_{(002)} \approx 3.55 \text{ \AA}$. In addition, in both samples synthesized using FeCl_3 , a number of additional peaks are identified as the Fe_3O_4 iron oxide (magnetite) phase.

2. The AC2 biocarbon is characterized by a microporous structure in which a significant volume fraction (about 35%) is made by pores of 2.2 and 5.0 nm radii. A significant increase in the fraction of pores with radii from 5 to 30 nm and a decrease in the proportion of pores with radii greater than 30 nm can be detected in the AC1 sample. However, an analysis of the pore radius distribution functions showed that the average pore radii in the AC2 and AC1 samples were almost indistinguishable (4.25 and 4.05 nm, respectively). The analysis of the integral scattering characteristics (invariant and Porod constant) reveals significant differences of these values depending on the mode of sample processing. Thus, AC0 carbon has the smallest specific area of $212 \text{ m}^2\cdot\text{cm}^{-3}$, AC1 carbon is slightly larger in $280 \text{ m}^2\cdot\text{cm}^{-3}$, and AC2 has the largest specific surface area of $480 \text{ m}^2\cdot\text{cm}^{-3}$.

3. A study of the adsorption isotherms of methylene blue showed that AC2 biocarbon has significantly better adsorption properties compared to AC0 and AC1. Analysing the shape of the isotherms, we can say that all isotherms belong to the second type of adsorption isotherms, which indicates the presence in the analysed biocarbons along with micropores also a certain number of meso- and macropores. The Langmuir constant K , which is the equilibrium constant of the adsorption process, decreases with increasing carbon adsorption capacity. This means that AC2 carbon has a significantly smaller proportion of large pores compared to AC0 and AC1 carbon, and is dominated by micropores.

4. As a result of the magnetic measurements, the hysteresis loops for the AC1 and AC2 magnetic biocarbon were obtained. Based on the obtained data, the coercive force (H_c), the specific saturation magnetization (σ_s), the residual specific magnetization (σ_r), the relative residual magnetization (σ_r/σ_s) were calculated. Taking into account the dependence of the coercive force on the particle diameter in the Fe_3O_4 dispersions, for the measured values of the coercive force, the average size of the magnetic moment carriers was 30 nm for the AC2 sample and 50 nm for the AC1 sample.

REFERENCE

- ABIOUE A.M., ANI F.N. 2015. Recent development in the production of activated carbon electrodes from agricultural waste biomass for supercapacitors: A review. *Renewable and Sustainable Energy Reviews*. Vol. 52 p. 1282–1293. DOI 10.1016/j.rser.2015.07.129.
- APAEV B.A. 1973. Fazoviy mahnitnyy analiz splavov [Phase magnetic analysis of alloys]. Moskva. Metallurhiya pp. 280.
- BESTANI B., BENDERDOUCHE N., BENSTAALI B., BELHAKEM M., ADDOU A. 2008. Methylene blue and iodine adsorption onto an activated desert plant. *Bioresource Technology*. Vol. 99. Iss. 17 p. 8441–8444. DOI 10.1016/j.biortech.2008.02.053.
- BUHAENKO I.F. 2007. Obschaya tekhnolohiya otrasli. Nauchnie osnovy tekhnolohii sakhara. Ch.st 1. Uchebnik dlya studentov vuzov [General technology of the industry. Scientific basis of sugar technology. Part 1. Textbook for university students]. Sankt Petersburg: Giord, Ao. ISBN 978-5-98879-025-9 pp. 512.
- COEY J.M.D. 2010. Magnetism and magnetic materials. Cambridge. Cambridge Univ. Press. ISBN 9780521816144 pp. 625.
- DOBELE G., DIZHBITE T., GIL M.V., VOLPERTS A., CONTENO T.A. 2012. Production of nanoporous carbons from wood processing wastes and their use in supercapacitors and CO_2 capture. *Biomass and Bioenergy*. Vol. 46. p. 145–154. DOI 10.1016/j.biombioe.2012.09.010.
- GONZALEZ-GARCIA P. 2018. Activated carbon from ligninocellulose precursors: A review of the synthesis methods, characterization techniques and applications. *Renewable and Sustainable Energy Reviews*. Vol. 82 p. 1393–1414.
- GOYA G.F., BERQUO T.S., FONSECA F.S. 2003. Static and dynamic magnetic properties of spherical magnetite nanoparticles. *Journal of Applied Physics*. Vol. 94. Iss. 5 p. 3520–3528. DOI 10.1063/1.1599959.
- HSIEH C.-T., TENG H. 2000. Influence of mesopore volume and adsorbate size on adsorption capacities of activated carbons in aqueous solutions. *Carbon*. Vol. 38 p. 863–869.
- HUBIN S.P., KOKSHAROV YU.A., KHOMUTOV H.B., YURKOV H.YU. 2005. Mahnitnye nanochasticy: metody polucheniya, stroeniya i svoystva [Magnetic nanoparticles: methods of obtaining, structure and properties]. *Uspehi khimii*. Vol. 74. Iss. 6 p. 539–574. DOI 10.1070/RC2005v074n06ABEH 000897.
- IOANNIDOU O., ZABANIOTOU A. 2007. Agricultural residues as precursors for activated carbon production – A review. *Renewable and Sustainable Energy Reviews*. Vol. 11 p. 1966–2005. DOI 10.1016/j.rser.2006.03.013.
- KADIRVELU K., KAVIPRIYA M., KARTHIKA C., RADHIKA M., VENNILAMANI N., PATTABHI S. 2003. Utilization of various agricultural wastes for activated carbon preparation and application for removal of dyes and metal ions from aqueous solutions. *Bioresource Technology*. Vol. 87 p. 129–132. DOI 10.1016/S0960-8524(02)00201-8.
- KIM B.C., LEE J., UM W., KIM J., JOO J., LEE J.H., KWAK J.H., KIM J.H., LEE C., LEE H., ADDLEMAN R.S., HYEON T., GU M.B., KIM J. 2011. Magnetic mesoporous materials for removal of environmental wastes. *Journal of Hazardous Materials*. Vol. 192. Iss. 3 p. 1140–1147. DOI 10.1016/j.jhazmat.2011.06.022.
- KONDIR A.I., BORYSYUK A.K., PAZDRIY I.P., SHWACHKO S.H. 2004. Zastosuvannya mahnitometra dlya fazovoho analizu specialnikh staley ta splaviv [Application of a magnetometer for phase analysis of special steels and alloys]. *Vibracii v tekhnice i tekhnolohiyakh*. No. 2 (34) p. 41–43.
- LIE W.-J., TIAN K., HE Yr., JIANG H., YU H.-Q. 2014. High-yield harvest of nanofibers/mesoporous carbon composite by pyrolysis of waste biomass and its application for high durability electrochemical energy storage. *Environmental Science and Technology*. Vol. 48. Iss. 23. p. 13951–13959. DOI 10.1021/es504184c.
- LOWELL S., SHIELDS J.E. 1998. Powder surface area and porosity. Kluwer (reprinted – London: Chapman & Hall) 3rd ed. ISBN 9780412396908 pp. 252.
- OLIVEIRA L.C.A., PEREIRA E., GUIMARAES I.R., VALLONE A., PEREIRA M., MESQUITA J.P., SAPAG K. 2009. Preparation of activated carbons from coffee husks utilizing FeCl_3 and ZnCl_2 as activating agents. *Journal of Hazardous Materials*. Vol. 165. Iss. 1–3 p. 87–94. DOI 10.1016/j.jhazmat.2008.09.064.
- PAKHOVCHISHIN S.V., CHERNISH I., HRYZENKO V. 1991. Nekotorye ohranicheniya primeneniya indikatornoho metoda pri izuchenii poverkhnosti chastic hrafita [Some restrictions on the use of the indicator method for studying the surface of graphite particles]. *Kolloidnyy Zhurnal*. Vol. 53. Iss. 2 p. 284–289.
- SAMAR K., MUTHANNA J. 2012. Optimization of preparation conditions for activated carbons from date stones using response surface methodology. *Powder Technology*. Vol. 224 p. 101–108. DOI 10.1016/j.powtec.2012.02.037.
- SPICHAK V.V., VRATSKIY A.M. 2012. Suchasni napryamki vykoristanna ta utylizacii buryakovoho zhomu [Modern directions of use and utilization of beet pulp]. *Visnyk cukrovykiv Ukrainy*. No. 2 (69) p. 13–15.
- THEYDAN S.K., AHMED M.J. 2012. Adsorption of methylene blue onto biomass-based activated carbon by FeCl_3 activation: Equilibrium, kinetics, and thermodynamic studies. *Journal of Analytical and Applied Pyrolysis*. Vol. 97 p. 116–122. DOI 10.1016/J.JAAP.2012.05.008.
- VERVIKISHKO D.E., YANILKIN I.V., DOBELE G.V., VOLPERTS A., ATAMANYUK I.N., SAMETOV A.A., SHKOLNIKOV E.I. 2015. Activated carbon for supercapacitor electrodes with an aqueous electrolyte. High temperature. Vol. 53. Iss. 5 p. 758–764. DOI 10.1134/S0018151X15050272.
- WANG T., LIANG L., WANG R., JIANG Y., LIN K., SUN J. 2012. Magnetic mesoporous carbon for efficient removal of organic

- pollutants. *Adsorption*. Vol. 18. Iss. 5–6 p. 439–444. DOI 10.1007/s10450-012-9430-2.
- XIAO-FEI T., SHAO-BO L., YUN-GUO L., YAN-LING G., GUANG-MING Z., XINJIANG H., SHAO-HENG L., LU-HUA J. 2017. Biochar as potential sustainable precursors for activated carbon production: Multiple applications in environmental protection and energy storage. *Bioresource Technology*. Vol. 227 p. 359–372. DOI 10.1016/j.biortech.2016.12.083.
- YAHYA M.A., AL-QODAHB Z., NGAH C.W.Z. 2015. Agricultural bio-waste as potential precursors for activated carbon production: A review. *Renewable and Sustainable Energy Reviews*. Vol. 46 p. 218–235. DOI 10.1016/j.rser.2015.02.051.
- YANG H., OGAWA T., HASEGAWA D., TAKAHASHI M. 2008. Synthesis and magnetic properties of monodisperse magnetite nanocubes. *Journal of Applied Physics*. Vol. 103. Iss. 7 p. 07D526-1–07D526-3. DOI 10.1063/1.2833820.
- ZHU X., FENG Q., YUCHEN L., MATERA D., GANG WU, SHICHENG ZH., JIAN-MIN CH. 2016. Controllable synthesis of magnetic carbon composites with high porosity and strong acid resistance from hydrochar for efficient removal of organic pollutants: An overlooked influence. *Carbon*. Vol. 99 p. 338–347. DOI 10.1016/j.carbon.2015.12.044.